

1 Global Sensitivity of Tropospheric Ozone to Precursor Emissions in

2 Clean and Present-Day Atmospheres: Insights from AerChemMIP

3 Simulations

4 Wei Wang¹ and Chloe Yuchao Gao^{2,3,*}

⁵ ¹ Nanjing-Helsinki Institute in Atmospheric and Earth System Sciences, Nanjing
⁶ University, Nanjing, 210023, China

7 ² Department of Atmospheric and Oceanic Sciences & Shanghai Key Laboratory of
8 Ocean-Land-Atmosphere Boundary Dynamics and Climate Change, Fudan
9 University, Shanghai, 200438, China

¹⁰ ³ Institute of Eco-Chongming (IEC), Shanghai, China

11

12 * Corresponding author: Chloe Yuchao Gao (gyc@fudan.edu.cn)

13 **Abstract**

14 Ozone (O_3) is a Short-lived Climate Forcer (SLCF) that contributes to radiative
15 forcing and indirectly affects the atmospheric lifetime of methane, a major
16 greenhouse gas. This study investigates the sensitivity of global O_3 to precursor
17 gases in a clean atmosphere, where hydroxyl (OH) radical characteristics are more
18 spatially uniform than in present-day conditions, using data from the *PiClim*
19 experiments of the Aerosols and Chemistry Model Intercomparison Project
20 (AerChemMIP) within the CMIP6 framework. We also evaluate the O_3 simulation
21 capabilities of four Earth system models (CESM2-WACCM, GFDL-ESM4,
22 GISS-E2-1-G, and UKESM1-0-LL). Our analysis reveals that the CESM and GFDL
23 models effectively capture seasonal O_3 cycles and consistently simulate vertical O_3
24 distribution. While all models successfully simulate O_3 responses to anthropogenic
25 precursor emissions, CESM and GFDL show limited sensitivity to enhanced natural
26 NO_x emissions (e.g., from lightning) compared to GISS and UKESM. The
27 sensitivities of O_3 to its natural precursors (NO_x and VOCs) in GISS and UKESM
28 models are substantially lower than their responses to anthropogenic emissions,
29 particularly for lightning NO_x sources. These findings refine our understanding of
30 O_3 sensitivity to natural precursors in clean atmospheres and provide insights for
31 improving O_3 predictions in Earth system models.

32 **1 Introduction**

33 Tropospheric ozone (O_3) is a key air pollutant and atmospheric oxidant,
34 exerting extensive influence on air quality and human health (Coffman et al., 2024;
35 Lim et al., 2019; Malley et al., 2017; Nuvolone et al., 2018), climate systems, and
36 biogeochemical processes (Hu et al., 2023; Fowler et al., 2009). As a Short-lived
37 Climate Forcer (SLCF), tropospheric O_3 exerts a radiative forcing of 0.35–0.5 W
38 m^{-2} and influences atmospheric processes such as evaporation, cloud formation, and
39 general circulation (Khomsi et al., 2022; Möller and Mauersberger, 1992; Rogelj et
40 al., 2014; Stevenson et al., 2013). Furthermore, O_3 plays a crucial role in regulating
41 the terrestrial carbon sink and enhancing the formation of the hydroxyl (OH) radical
42 (Naik et al., 2013b), which, in turn, affect the lifetime of methane (and halocarbons),
43 the second most prominent anthropogenic greenhouse gas after carbon dioxide
44 (KumAŞ et al., 2023). O_3 also contributes to an increased atmospheric oxidation
45 capacity, influencing the formation of secondary aerosols, such as organic aerosol,
46 sulfate, and nitrate, which have significant implications for radiative forcing (Karsel
47 et al., 2018).

48 While stratospheric O_3 entrainment contributes to tropospheric O_3 levels, the
49 primary source of tropospheric O_3 is photochemical production. This secondary
50 pollutant is formed through photochemical oxidation reactions involving oxides of
51 nitrogen ($NO + NO_2 = NO_x$) and volatile organic compounds (VOCs) in the
52 presence of OH and hydroperoxyl (HO_2) radicals (Monks et al., 2015). The
53 relationship between O_3 and its precursors is nonlinear, making it challenging to
54 mitigate O_3 pollution through simple precursor reduction strategies. Regional-scale
55 sensitivity to O_3 precursors has been extensively investigated, such as emphasizing
56 the diagnostic utility of ratios including O_3/NO_x (Jin et al., 2023; Sillman and He,
57 2002) and VOC/NO_x (Li et al., 2024) for assessing O_3 - NO_x -VOC sensitivity, and
58 nations such as the United Kingdom and the United States have demonstrated
59 significant success in controlling regional ozone levels by implementing measures
60 to reduce NO_x emissions (Hakim et al., 2019). However, the global-scale sensitivity
61 of O_3 to its precursors has received limited attention, despite evidence suggesting
62 that global O_3 forcing may have a more substantial impact on climate forcing than
63 localized O_3 enhancements. Consequently, improving our understanding of O_3

64 formation mechanisms on a global scale is essential for effective air quality
65 management and climate change mitigation strategies (Yu et al., 2021).

66 Recent studies utilizing Coupled Model Intercomparison Project Phase 6
67 (CMIP6; Eyring et al., 2016) datasets have offered insights into the spatio-temporal
68 evolution of the global tropospheric O₃ budget from 1850 to 2100 (Griffiths et al.,
69 2021; Turnock et al., 2019) and have quantified the global stratosphere-troposphere
70 O₃ exchange process (Li et al., 2024; Griffiths et al., 2021). However, challenges
71 persist in quantifying the sensitivity of global O₃ to its precursors when assessing
72 the increasing global O₃ forcing attributed to these precursors. These challenges
73 arise from regional variability in meteorological conditions (Carrillo-Torres et al.,
74 2017), differences in NO_x and VOC volume mixing ratios (Jin et al., 2023; Sillman
75 and He, 2002), and the distinct characteristics of hydroxyl radical (OH) and
76 hydroperoxyl radical (HO₂⁻) influenced by varying degrees of urbanization (Karl et
77 al., 2023; Vermeuel et al., 2019). Furthermore, while the observed upward trends in
78 O₃ levels are primarily attributed to increased precursor emissions, limited research
79 has investigated whether contemporary atmospheric conditions—shaped by climate
80 warming and enhanced oxidation capacities—may be creating a more favorable
81 environment for O₃ formation.

82 To address these gaps, this study investigates the sensitivity of global-scale O₃
83 to its precursors under a pre-industrial background atmosphere, with approximate
84 unified HO_x conditions in major continental areas. We also examine the feedback
85 mechanisms of different model responses to precursors from both anthropogenic
86 and natural sources, using *PiClim* experiment data from the Aerosols and Chemistry
87 Model Intercomparison Project (AerChemMIP) simulations (Collins et al., 2017)
88 within CMIP6. Additionally, this research evaluates the ozone formation potential
89 in the pre-industrial era based on contemporary (2014) emissions of O₃ precursors,
90 with the aim of elucidating whether shifts in the background atmosphere have
91 rendered it chemically more conducive to O₃ generation. Our analysis employs four
92 models with interactive stratospheric and tropospheric chemistry, which have been
93 extensively utilized in O₃-related research (Brown et al., 2022; Griffiths et al., 2021;
94 Tilmes et al., 2022; Zeng et al., 2022). This approach allows us to assess the
95 global-scale sensitivity of O₃ to its precursors, evaluate the consistency and
96 discrepancies among different models in representing O₃-precursor relationships,

97 and provide insights into the potential impacts of changing emissions on future
98 global O₃ levels and associated climate forcing, contributing to more accurate
99 projections of future climate change.

100 **2 Models and methods**

101 **2.1 Model descriptions**

102 We use monthly-mean simulation data from four Earth system models in this
103 study. The four chosen models possess the benefit of extensive applicability and a
104 comprehensive *PiClim* experimental framework. Table 1 summarizes key model
105 features, including model resolution, vertical stratification, complexity of gas-phase
106 chemistry, and relevant references. All models include interactive coupling of
107 tropospheric and stratospheric chemistry with O₃ dynamics integrated into the
108 radiation scheme, simulating the interaction between O₃ concentration and
109 temperature. The response of simulated reactive gas emissions to chemical
110 complexity is important. For example, changes in Biogenic Volatile Organic
111 Compounds (BVOCs) can impact O₃, methane lifetime, and potentially the
112 oxidation of other aerosol precursors in models with interactive tropospheric
113 chemistry.

Table 1. Information on model resolution, vertical levels, property of gas-phase chemistry and references.

Model	Resolution (lat × lon)	Vertical levels	Tropospheric and stratospheric chemistry	Aerosol model	Simulation reference
CESM2-WACCM	192 × 288	70 levels; top level 6×10^{-6} hPa		MAM4	(Gettelman et al., 2019)
GFDL-ESM4	180 × 288	49 levels; top level 0.01 hPa	Interactive	MATRIX	(Dunne et al., 2020; Horowitz et al., 2020)
GISS-E2-1-G	90 × 144	40 levels; top level 0.1 hPa		OMA	(Miller et al., 2014; Kelley et al., 2020)
UKESM1-0-LL	144 × 192	85 levels; top level 1 hPa		GLOMAP	(Mulcahy et al., 2018; Sellar et al., 2019)

116 CESM2-WACCM (hereafter “CESM”) is a fully coupled Earth system model
117 that integrates the Community Earth System Model version 2 (Emmons et al., 2020)
118 with the Whole Atmosphere Community Climate Model version 6 (WACCM6). The
119 atmospheric component operates at a horizontal resolution of 0.9375° latitude by
120 1.25° longitude, with 70 hybrid sigma-pressure vertical layers extending from the
121 surface to 6×10^{-6} hPa. Its interactive chemistry and aerosol modules include the
122 troposphere, stratosphere, and lower thermosphere, with a comprehensive treatment
123 of 231 species, 150 photolysis reactions, 403 gas-phase reactions, 13 tropospheric
124 heterogeneous reactions, and 17 stratospheric heterogeneous reactions (Emmons et
125 al., 2020). The model utilizes the four-mode Modal Aerosol Model (MAM4)
126 (Emmons et al., 2020) and features its secondary organic aerosol (SOA) framework
127 based on the Volatility Basis Set (VBS, Donahue et al., 2013) approach. The
128 photolytic calculations use both inline chemical modules and a lookup table
129 approach, which does not consider changes in aerosols.

130 The Atmospheric Model version 4.1 (AM4.1, Horowitz et al. (2020)) within
131 the GFDL Earth system model (Dunne et al., 2020) incorporates an interactive
132 chemistry scheme that spans both the troposphere and stratosphere (GFDL-ESM4;
133 hereafter “GFDL”). The atmospheric component operates at a horizontal resolution
134 of 1° latitude by 1.25° longitude, with 49 hybrid sigma-pressure vertical layers
135 extending from the surface to 0.01 hPa. This scheme includes 56 prognostic tracers,
136 36 diagnostic species, 43 photolysis reactions, 190 gas-phase kinetic reactions, and
137 15 heterogeneous reactions. Stratospheric chemistry accounts for key O_3 depletion
138 cycles (O_x , HO_x , NO_x , ClO_x , and BrO_x) and heterogeneous reactions on
139 stratospheric aerosols (Austin et al., 2013). Photolysis rates are calculated
140 dynamically with the FAST-JX version 7.1 code, which considers the radiative
141 impacts of modeled aerosols and clouds. The chemical mechanism is further
142 elaborated in Horowitz et al. (2020), and the gas-phase and heterogeneous chemistry
143 are similar to those employed by Schnell et al. (2018). Non-interactive natural
144 emissions of O_3 precursors are prescribed as outlined in Naik et al. (2013a).

145 The GISS model, developed by the NASA Goddard Institute for Space Studies,
146 integrates the chemistry-climate model version E2.1 with the GISS Ocean v1 (G01)
147 model (GISS-E2-1-G; hereafter “GISS”). The specific configurations of this model

148 utilized for the CMIP6 are detailed in Kelley et al. (2020). In this study, we focus on
149 the model subset that includes online interactive chemistry. The atmospheric
150 component operates at a horizontal resolution of 2° latitude by 2.5° longitude, with
151 40 hybrid sigma-pressure vertical layers extending from the surface to 0.1 hPa. The
152 interactive chemistry module employs the GISS Physical Understanding of
153 Composition-Climate Interactions and Impacts (G-PUCCINI) mechanism for
154 gas-phase chemistry (Kelley et al., 2020; Shindell et al., 2013). For aerosols, the
155 model utilizes either the One-Moment Aerosol (OMA) or the Multiconfiguration
156 Aerosol Tracker of Mixing state (MATRIX) model (Bauer et al., 2020). The
157 gas-phase chemistry involves 146 reactions, including 28 photodissociation
158 reactions, affecting 47 species across the troposphere and stratosphere, along with
159 an additional five heterogeneous reactions. The model transports 26 aerosol particle
160 tracers and 34 gas-phase tracers (OMA).

161 UKESM represents the United Kingdom's Earth system model (Sellar et al.,
162 2019). It builds upon the Global Coupled 3.1 (GC3.1) configuration of HadGEM3
163 (Williams et al., 2018), incorporating additional Earth system components, such as
164 ocean biogeochemistry, the terrestrial carbon-nitrogen cycle, and atmospheric
165 chemistry (UKESM1-0-LL; hereafter "UKESM"). Walters et al. (2019) provided
166 descriptions of the atmospheric and land components. The atmospheric component
167 operates at a horizontal resolution of 1.25° latitude by 1.875° longitude, with 85
168 vertical layers extending from the surface to 85 km. The chemistry module in the
169 UKESM model is a unified stratosphere-troposphere scheme (Archibald et al., 2020)
170 including 84 tracers, 199 bimolecular reactions, 25 unimolecular and termolecular
171 reactions, 59 photolytic reactions, 5 heterogeneous reactions, and 3 aqueous-phase
172 reactions for the sulfur cycle from the United Kingdom Chemistry and Aerosols
173 (UKCA) model. The aerosol module is based on the two-moment scheme from
174 UKCA, known as GLOMAP mode, and is integrated into the Global Atmosphere
175 7.0/7.1 configuration of HadGEM3 (Walters et al., 2019). The UKESM uses
176 interactive Fast-JX photolysis scheme, which is applied to derive photolysis rates
177 between 177 and 850 nm, as described in Telford et al. (2013). In the lower
178 mesosphere, photolysis rates are calculated using lookup tables (Lary and Pyle,
179 1991).

180 Models differ in their representation of O₃ source and sink processes, as well as
181 in the definitions of the associated budget terms, which contributes to variability in
182 model outcomes (Stevenson et al., 2006; Young et al., 2018). For example, in the
183 GISS model, the tropospheric chemistry component simulates the
184 NO_x-HO_x-O_x-CO-CH₄ system and the oxidation pathways for non-methane volatile
185 organic compounds (NMVOCs). Central to these discrepancies are the treatments of
186 non-methane volatile organic compound NMVOCs chemistry, which impacts both
187 chemical production and destruction rates, along with surface removal mechanisms
188 and stratospheric influences. Furthermore, the choice of tropopause definition can
189 significantly alter the diagnosed O₃ burden, as well as the flux from the stratosphere.

190 All four of the interactive tropospheric chemistry models contain
191 parameterizations of the nitrogen oxide (NO_x) emissions from lightning based on
192 the height of the convective cloud top (Price et al., 1997; Price and Rind, 1992;
193 Price, 2013), and the tropopause height for each model based on the WMO
194 definition. Each model has a different way of implementing emissions and how
195 much they are profiled. For instance, online calculations of lightning NO_x emissions
196 during deep convection in the GISS model are based on the method described by
197 (Kelley et al., 2020). Lightning NO_x continues to be a major source of uncertainty in
198 both model comparisons and the temporal development of tropospheric O₃ because
199 it has a disproportionately significant influence on tropospheric-O₃ concentration
200 relative to surface emissions (Murray et al., 2013).

201 BVOC emissions are modeled as a function of vegetation type and cover, as
202 well as temperature and photosynthetic rates (gross primary productivity) (Unger,
203 2014; Sporre et al., 2019; Pacifico et al., 2011; Guenther et al., 1995). While models
204 vary in the speciation of emitted VOCs, they commonly include isoprene and
205 monoterpenes, each with its own distinct emission parameterization. Despite the
206 common reliance on photosynthetically active radiation for the parameterization of
207 BVOC emissions across the four models, there exist notable distinctions. For
208 instance, the GFDL model exclusively considers the leaf area index, neglecting the
209 impact of temperature on BVOC emissions, and the CESM, GISS, and UKESM
210 models omit the influence of vegetation type from their calculations.

211 **2.2 Simulation data and experimental design**

212 The primary objective of AerChemMIP is to quantitatively ascertain the
213 influence of aerosols and reactive trace gases on the climate system, as well as the
214 bidirectional feedback mechanisms involved (Collins et al., 2017). Table 2 presents
215 a synopsis of the experimental configurations employed in this study. The control
216 experiment, denoted as *PiClim-control*, is designed to stabilize both atmospheric
217 composition and climatic conditions at a state reminiscent of the pre-industrial era,
218 specifically 1850. The *PiClim-2x* experiment involves doubling of individual
219 natural emission fluxes relative to the 1850 control, while the *PiClim-x* experiments
220 calibrate these fluxes to align with the emission levels prevalent in 2014 (Collins et
221 al., 2017). *PiClim-2xNO_x* represents the nitric oxide emissions from natural sources
222 due to lightning activity doubles. *PiClim-2xVOC* represents the volatile organic
223 compound emissions from natural sources, including isoprene and monoterpenes,
224 doubles. *PiClim-VOC* represents the pre-industrial climatological control with 2014
225 VOC emissions both from anthropogenic and natural sources. *PiClim-aer* represents
226 the pre-industrial climatological control with 2014 aerosol concentrations. *HC*
227 represents halocarbons include CFCs, HCFCs and compounds containing bromine.
228 *NTCF* represents near-term climate forcers, including aerosols and chemically
229 reactive gases such as tropospheric ozone and methane. *BC* represents black carbon
230 and *N₂O* represents nitrous oxide.

Table 2. The available experiments of selected models in this study. "X" represents the experiment is available

Model	<i>piClim-2x</i> <i>NO_x</i>	<i>piClim-2x</i> <i>VOC</i>	<i>piClim-</i> <i>HC</i>	<i>piClim-</i> <i>CH₄</i>	<i>piClim-</i> <i>NO_x</i>	<i>piClim-</i> <i>VOC</i>	<i>piClim-</i> <i>TCF</i>	<i>piClim-</i> <i>N₂O</i>	<i>piClim</i> <i>-O₃</i>	<i>piClim-</i> <i>aer</i>	<i>piClim-co</i> <i>ntrol</i>	<i>piClim</i> <i>-BC</i>
CESM2-W ACCM	X	X	X	X	X	X	X	X	X			
GFDL-ESM 4	X	X	X		X	X			X	X	X	X
GISS-E2-1- G	X	X	X	X	X	X	X	X	X	X	X	X
UKESM1-0- LL	X	X	X	X	X	X	X	X	X	X	X	X

233 We analyzed models that had archived sufficient data in the Earth System Grid
234 Federation (ESGF) system to permit accurate characterization of tropospheric O₃. In
235 practice this meant we used archived O₃ data from the AERmon characterization of
236 the tropospheric O₃ (variable name: “o3”) on native model grids. Other variables
237 used include chemical production (variable name: “o3prod”), chemical destruction
238 (variable name: “o3loss”), nitrogen monoxide (variable name: “no”), nitrogen
239 dioxide (variable name: “no2”), isoprene (variable name: “isop”), organic dry
240 aerosol (variable name: “emioa”), and secondary organic aerosol (variable name:
241 “mmrsoa”). All data used in this paper are available on the Earth System Grid
242 Federation website and can be downloaded from
243 <https://esgf-index1.ceda.ac.uk/search/cmip6-ceda/> (last access: 4 July 2024,
244 ESGF-CEDA, 2020).

245 A new set of historical anthropogenic emissions has been developed with the
246 Community Emissions Data System (CEDS, Hoesly et al., 2018). CEDS uses
247 updated emission factors to provide monthly emissions of the major aerosol and
248 trace gas species over the period 1750 to 2014 for use in CMIP6, and biomass
249 burning emissions are based on a different inventory developed separate from
250 CEDS (Van Marle et al., 2017). The primary analysis examines emissions of NO_x
251 and VOCs from anthropogenic (Hoesly et al., 2018) and biomass burning sources
252 (van Marle et al., 2017) that were provided as a common emission inventory to be
253 used by all models (including the four in this study) in CMIP6 simulations. In the
254 CESM and GFDL models, biogenic emissions, including isoprene and
255 monoterpenes, are calculated interactively using MEGAN version 2.1 (Guenther et
256 al., 2012) and are further utilized for SOA formation. While in the GISS model,
257 biogenic emissions of isoprene are computed online and are sensitive to temperature
258 (Shindell et al., 2006), whereas alkenes, paraffins, and terpenes are prescribed. And
259 in the UKESM model, emissions of isoprene and monoterpenes are interactively
260 calculated using the iBVOC emission model (Pacifico et al., 2011).

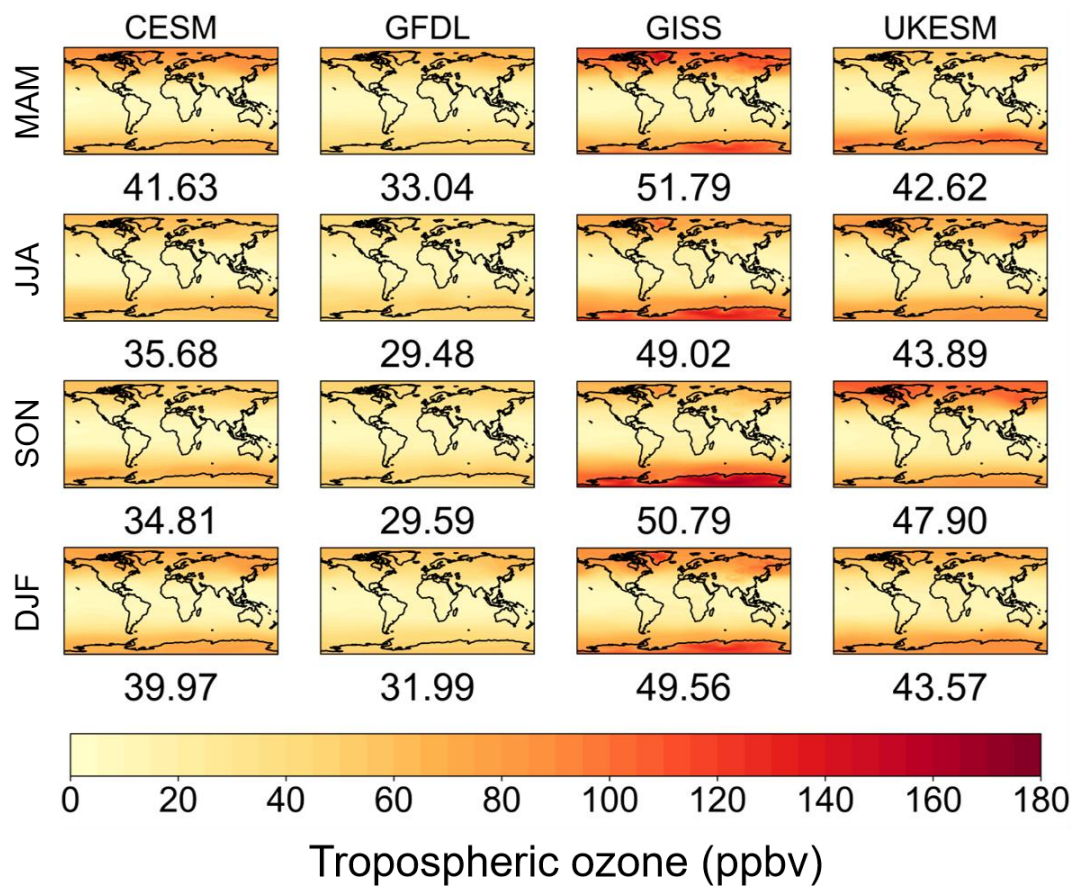
261 **3 Results and Discussions**

262 **3.1 Spatial, seasonal, and vertical distribution of tropospheric O₃**

263 We first investigate the seasonal and vertical variations of ozone volume
264 mixing ratio in the pre-industrial atmospheres simulated by four selected models.

265 The analysis of tropospheric O₃ data derived from the *PiClim* experiment outcomes
266 of CMIP6 models reveals distinct seasonal cycles and inter-model variations (Fig.
267 1). The GISS model demonstrates the highest simulated tropospheric column O₃
268 volume mixing ratio at 50.29 ppbv in the 29th and 30th year of simulation, followed
269 by the UKESM (44.50 ppbv), CESM (38.02 ppbv), and GFDL (31.03 ppbv), where
270 the height of the tropopause is based on the definition of WMO. These are
271 consistent with previous findings from historical experiments (Griffiths et al.,
272 2021).

273 Furthermore, our analysis indicates that the disparity in O₃ volume mixing ratio
274 during the *PiClim* experiment primarily occurs in polar regions. This may be
275 attributed to the GISS model's ability to replicate a more robust entrainment of
276 stratospheric O₃, a key source of tropospheric O₃ in the pre-industrial atmosphere,
277 particularly at the poles. Previous studies have demonstrated that elevated O₃ levels
278 in the Arctic during MAM and DJF, as well as in the Antarctic during JJA and SON,
279 result from the cumulative impact of the polar O₃ barrier (Hamlin and Honrath,
280 2002).



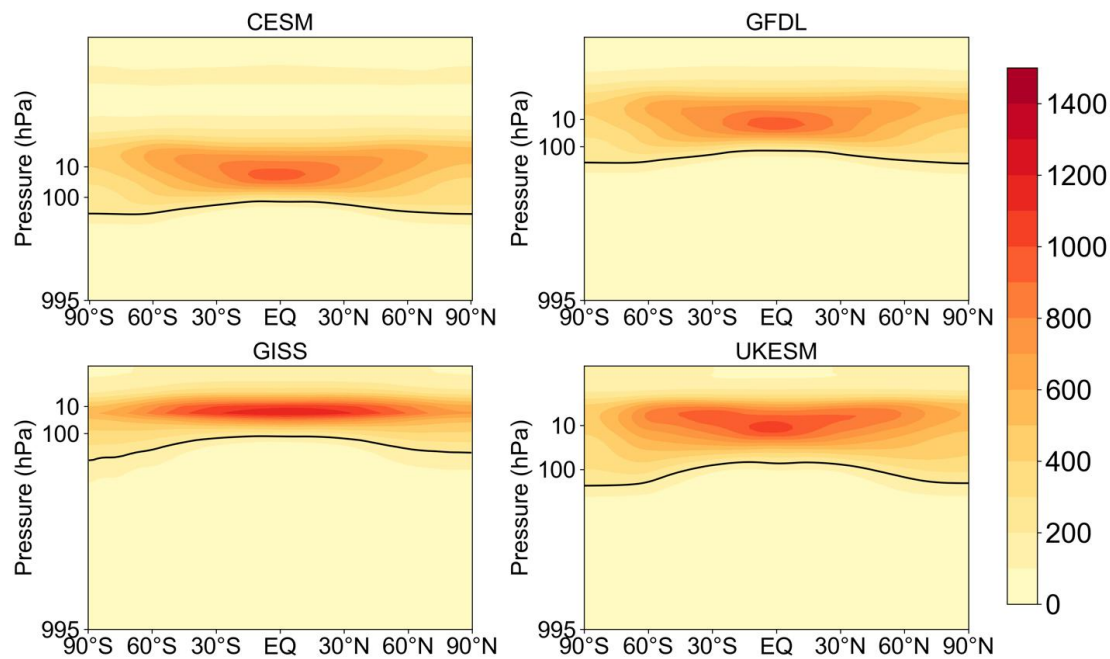
282 **Figure 1.** Comparison of the seasonal cycle of tropospheric column averaged
283 volume mixing ratio of O₃ of the *PiClim* experiment results in the 29th and 30th year
284 of simulation of the four models. Each row shows a separate meteorological season,
285 arranged from top to bottom: March to May (MAM), June to August (JJA),
286 September to November (SON), and December to February (DJF). Each column
287 represents a selected model, listed from left to right: CESM, GFDL, GISS, and
288 UKESM. The figures displayed below each chart represent the global average ozone
289 volume mixing ratio.

290 Seasonal variations in tropospheric O₃ volume mixing ratio exhibit
291 model-specific patterns. The CESM, GFDL, and GISS models simulate peak
292 tropospheric O₃ volume mixing ratio in spring during the *PiClim* experiments. In
293 contrast, the UKESM model reproduces maximum O₃ volume mixing ratio in
294 autumn, indicating a limited capability in simulating dynamic circulations in the
295 tropopause. Furthermore, the seasonal O₃ cycle simulations in CESM, GFDL, and
296 GISS exhibit distinct discrepancies in their outcomes. For instance, the CESM
297 model simulates the lowest O₃ volume mixing ratio in SON, while the GFDL model
298 exhibits the lowest volume mixing ratio in JJA. The GISS model simulation
299 indicates higher O₃ levels in autumn compared to DJF, which is consistent with
300 results from historical experiments (Griffiths et al., 2021). Additionally, our analysis
301 reveals that the CESM simulations demonstrate the most pronounced seasonal
302 oscillation amplitude in O₃ volume mixing ratio, approximately 6.82 ppbv. This
303 feature underscores the model's sensitivity to seasonal factors affecting tropospheric
304 O₃ dynamics.

305 In the *PiClim* experiments, all four models accurately reproduce the peak
306 volume mixing ratio of O₃ in the middle stratosphere at 10 hPa and the zonal
307 average mixing ratios reaching their peak in the upper troposphere, particularly in
308 extratropical regions, indicative of extended chemical lifetimes at higher altitudes.
309 However, notable disparities are observed in the vertical distribution characteristics
310 of O₃ among the four models (Fig. 2). Specifically, the CESM model exhibits the
311 highest vertical extension, including an additional hotspot simulated in the
312 thermosphere. While the GFDL and CESM2 models exhibit consistent simulation
313 outcomes below 0.01 hPa, GISS and UKESM simulate significantly higher
314 stratospheric O₃ levels at 10 hPa in comparison.

315 Notable distinctions are observed in the spatial distribution of O₃. The GISS
316 model simulates a more vertically concentrated and latitudinally extended O₃

317 distribution. This characteristic may be a crucial factor contributing to the
 318 pronounced impact of O₃ transport in the polar stratosphere, as simulated by GISS.
 319 The zonal variability in O₃ distribution simulated by the UKESM falls between that
 320 of the GISS and CESM models. These inter-model discrepancies in O₃ simulation
 321 results likely reflect suboptimal representation of local and regional dynamics, as
 322 well as omitted chemical processes in corresponding models. The variability and
 323 uncertainty in O₃ precursor emission estimates further exacerbate these disparities.



324
 325 **Figure 2.** The zonal mean O₃ distribution for the 29th and 30th year of the *PiClim*
 326 experiment results from the (a) CESM, (b) GFDL, (c) GISS, and (d) UKESM model.
 327 Thick black lines represent the tropopause height for each model based on the
 328 WMO definition.

329 3.2 Characteristics of tropospheric O₃ under various experiments

330 Tables 3 and 4 present the global O₃ volume mixing ratio and tropospheric O₃
 331 volume mixing ratio across all experiments from the four different models. The
 332 GISS model simulations show higher tropospheric O₃ volume mixing ratios,
 333 reflecting increased rates of stratospheric downwelling and surface O₃ precursor
 334 emissions. However, its overall O₃ volume mixing ratio is notably lower compared
 335 to the UKESM, CESM, and GFDL models, with reductions of 114.24, 76.16, and
 336 47.04 ppbv, respectively. Analysis reveals that in the CESM, GFDL, and GISS
 337 models, the global O₃ molar fraction in the *PiClim-2NO_x* and *PiClim-NO_x*
 338 experiments surpasses that in the *PiClim-2VOC* and *PiClim-VOC* experiments. This
 339 difference is most pronounced in the GISS model, aligning with previous findings

340 indicating its heightened sensitivity to NO_x response (Turnock et al., 2019).
341 Conversely, in the UKESM model, the global O₃ molar fraction of the *PiClim-2NO_x*
342 experiment is lower than that of the *PiClim-2VOC* experiment. Interestingly, the
343 tropospheric O₃ volume mixing ratios in the *PiClim-2NO_x* experiment in the CESM
344 and GFDL models are notably lower than in their respective *PiClim-2VOC*
345 experiments, with reductions of 0.41 and 0.29 ppbv. This discrepancy challenges the
346 conventional understanding that increased NO_x emissions from lightning activity
347 should lead to tropospheric O₃ generation, suggesting a need for enhanced
348 sensitivity simulations in these two models regarding O₃ and NO_x emissions from
349 natural sources due to lightning activity. In contrast, the *PiClim-2NO_x* experiments
350 of the GISS and UKESM models effectively simulate an increase in tropospheric O₃
351 volume mixing ratio compared to their *PiClim-2VOC* experiments. Furthermore,
352 across all four models, the tropospheric O₃ volume mixing ratio of the *PiClim-NO_x*
353 experiment surpasses that of the *PiClim-VOC* experiment, indicating the models'
354 ability to accurately replicate the impact of rising anthropogenic emissions on O₃
355 production. Additionally, methane, a crucial natural source of volatile organic
356 compounds and a key greenhouse gas, enhances tropospheric O₃ generation by
357 influencing temperature, thereby elevating global O₃ volume mixing ratio. This
358 phenomenon contributes to the heightened sensitivity of O₃ to methane volume
359 mixing ratio in a clean atmosphere. Elevated volume mixing ratios of HCFCs
360 (*PiClim-HC*) and methane (*PiClim-CH₄*) lead to substantial stratospheric O₃
361 depletion, consequently affecting tropospheric O₃ volume mixing ratio through the
362 pod coil process. Other influencing factors, such as aerosols and black carbon,
363 induce warming through radiation effects, thereby simulating elevated O₃ volume
364 mixing ratio.

365 **Table 3.** The averaged concentrations of global ozone at all simulated vertical levels in the 29th and 30th year for each experiment of four models
 366 (ppbv).

Model	<i>piClim-2x</i> <i>NO_x</i>	<i>piClim-2x</i> <i>VOC</i>	<i>piClim-</i> <i>HC</i>	<i>piClim-</i> <i>CH₄</i>	<i>piClim-</i> <i>NO_x</i>	<i>piClim-</i> <i>VOC</i>	<i>piClim-</i> <i>TCF</i>	<i>piClim-</i> <i>N₂O</i>	<i>piClim</i> <i>-O₃</i>	<i>piClim-</i> <i>aer</i>	<i>piClim-co</i> <i>ntrol</i>	<i>piClim</i> <i>-BC</i>
CESM2-W ACCM	398.62	398.56	363.84	391.89	400.20	399.17	398.27	390.32				
GFDL-ESM 4	365.48	364.35	332.16		367.46	365.65			367.85	365.37	366.27	366.15
GISS-E2-1- G	322.97	317.19	278.06	324.52	322.51	316.40	320.04	310.42	319.19	320.09	318.92	318.96
UKESM1-0- LL	435.24	435.65	377.78	429.12	440.70	433.71	445.53	427.35	439.55	428.95	432.54	431.88

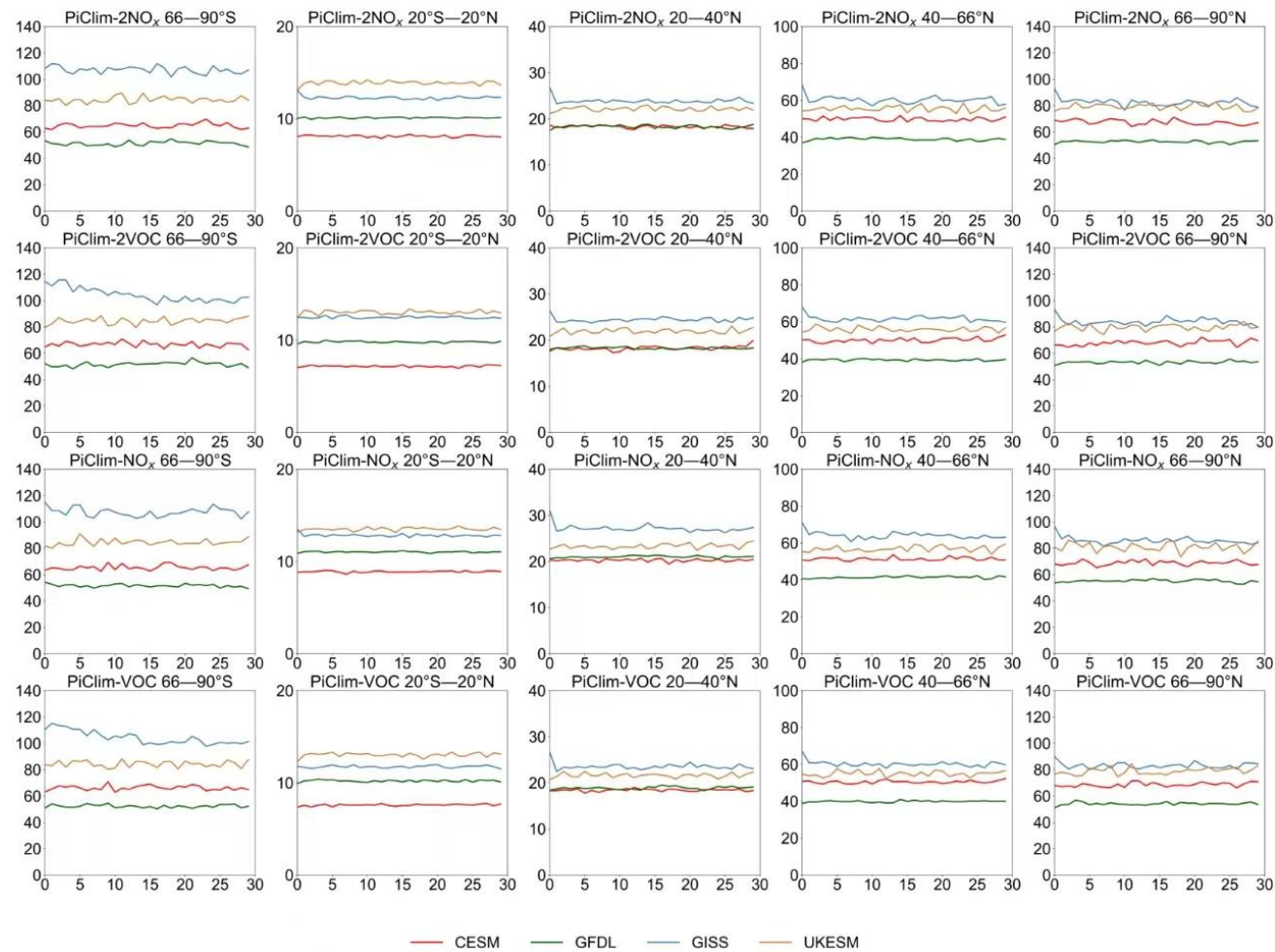
368

Table 4. The averaged concentrations of global tropospheric ozone in the 29th and 30th year for each experiment of four models (ppbv).

Model	<i>piClim-2x</i> <i>NO_x</i>	<i>piClim-2x</i> <i>VOC</i>	<i>piClim-</i> <i>HC</i>	<i>piClim-</i> <i>CH₄</i>	<i>piClim-</i> <i>NO_x</i>	<i>piClim-</i> <i>VOC</i>	<i>piClim-</i> <i>TCF</i>	<i>piClim-</i> <i>N₂O</i>	<i>piClim</i> <i>-O₃</i>	<i>piClim-</i> <i>aer</i>	<i>piClim-co</i> <i>ntrol</i>	<i>piClim</i> <i>-BC</i>
CESM2-W ACCM	38.17	38.58	33.44	39.42	39.16	39.14	41.33	38.10				
GFDL-ESM 4	31.33	31.62	24.42		32.64	32.25			34.09	31.01	30.79	30.95
GISS-E2-1- G	52.30	50.96	44.18	53.08	52.14	50.21	51.65	48.36	52.47	50.36	49.27	50.02
UKESM1-0- LL	47.53	46.14	31.04	45.55	46.02	45.97	47.29	45.04	46.65	43.69	46.70	45.11

369

370 Figure 3 shows the temporal evolution of tropospheric O₃ levels across various
371 latitudes, as simulated by four distinct models in O₃ precursor experiments. In the
372 *PiClim* experiments, none of the models predicted an enhancement in O₃ volume
373 mixing ratio, reflecting the consistent chemical lifetime of O₃ within the pristine
374 atmospheric conditions. However, discrepancies in O₃ predictions among the
375 models become more pronounced with increasing latitudes. While the CESM model
376 generally exhibits higher tropospheric O₃ volume mixing ratios compared to the
377 GFDL model, it paradoxically portrays the lowest O₃ levels in the equatorial region.
378 The GISS model demonstrates a marked disparity in tropospheric O₃ volume mixing
379 ratios between the Antarctic and Arctic regions, with the former registering notably
380 higher levels. In contrast, the CESM and GFDL models exhibit similar patterns in
381 this regard. A unique feature of the GISS model is a notable declining trend in
382 Antarctic tropospheric O₃ levels during the initial 15 years of both the *PiClim-2VOC*
383 and *PiClim-VOC* experiments. This trend is not observed in the CESM, GFDL, and
384 UKESM models, highlighting a distinctive characteristic of the GISS model's
385 simulation. The UKESM model stands out with its pronounced simulation of
386 elevated O₃ volume mixing ratios in the tropical belt. Furthermore, the
387 *PiClim-2xVOC* experiment conducted within the UKESM model demonstrates a
388 significant O₃ response to enhanced emissions of VOCs from natural sources in the
389 equatorial region. This suggests a strong sensitivity of O₃ in the UKESM to
390 increases in VOC emissions from natural sources.



391

Figure 3. The temporal evolution characteristics of annual mean tropospheric column averaged O₃ volume mixing ratio at different latitudes for each model are presented for the (a) *PiClim-2NO_x*, (b) *PiClim-2VOC*, (c) *PiClim-NO_x*, and (d) *PiClim-VOC* experiment.

394 **3.3 Analysis of O₃ generation in precursor experiments**

395 In the *PiClim* experiments, the O₃ production was defined as the cumulative
396 tendency from HO₂, CH₃O₂, RO₂, and NO reactions, while O₃ loss encompassed the
397 sum of O(1D) + H₂O, O₃ + HO₂, OH + O₃, and O₃ + alkene reactions. Figure 4
398 depicts the chemical production and consumption of tropospheric ozone in different
399 experiments of the four models. The GISS demonstrates the lowest O₃ chemical
400 production among the models, whereas the other three models show generally
401 consistent production levels. Notably, the GISS model exhibits a relatively low
402 efficiency in O₃ chemical consumptions, primarily due to missing the loss of O₃
403 with isoprene and terpenes process. The low offset of ozone production and
404 depletion in the pre-industrial atmosphere by the GISS model provides a new
405 perspective based on previous studies indicating the high offset of ozone production
406 and depletion in the present atmosphere by the GISS model. The four models all
407 showed high ozone chemical production in the *PiClim-NO_x* experiment, indicating
408 that the four all have perfect ability to simulate the photochemical generation
409 mechanism of tropospheric ozone. However, the CESM and GFDL models do not
410 show a significant increase in tropospheric O₃ chemical generation during the
411 *PiClim-2NO_x* experiment. And although the GISS and UKESM models successfully
412 simulated an increase in the O₃ chemical generation rate due to heightened lightning
413 activity in this experiment, these increases in ozone production are also much
414 smaller than the chemical production generated by the *PiClim-NO_x* experiment,
415 which might show that the theoretical mechanism of ozone sensitivity to natural
416 precursors in pre-industrial atmosphere differs from the present mechanism due to
417 the differences in the characteristics of intermediate products such as OH.
418 Furthermore, in either model, the ozone chemical production from the *PiClim-NO_x*
419 experiment, while higher than in other experiments other than *PiClim-NTCF*, is
420 much smaller than the ozone chemical production caused by this emission inventory
421 in the atmosphere today. Today's NO_x emission forcing has not led to a sustained
422 increase in the ozone volume mixing ratio in the pre-industrial atmosphere over a
423 long-time scale, which indicates important differences between the pre-industrial
424 atmosphere and the present atmosphere in terms of the ozone generation
425 environment and the ozone depletion environment.

Furthermore, the *PiClim-2VOC* experiment in the CESM and GFDL models lead to an increase in tropospheric O₃ volume mixing ratio, despite not reproducing higher O₃ chemical production. The UKESM model successfully captures the enhancement of O₃ chemical formation due to increased emissions of VOCs from natural sources, underscoring its precise sensitivity to these emissions and validating its capability to simulate O₃ dynamics influenced by them. However, the global O₃ volume mixing ratio in the *PiClim-2xVOC* experiment of these models is lower than that of the *PiClim-VOC* experiment. These observations illustrate the variability among models in capturing the O₃ response to its precursor species, stemming from varied treatments of critical atmospheric processes, including photolysis, dry deposition, transport mechanisms, and mixing dynamics. Furthermore, these findings highlight the variability in global O₃ sensitivity compared to local O₃ sensitivity, underscoring the complexity of studying O₃ sensitivity on a global scale to mitigate its climate impacts.

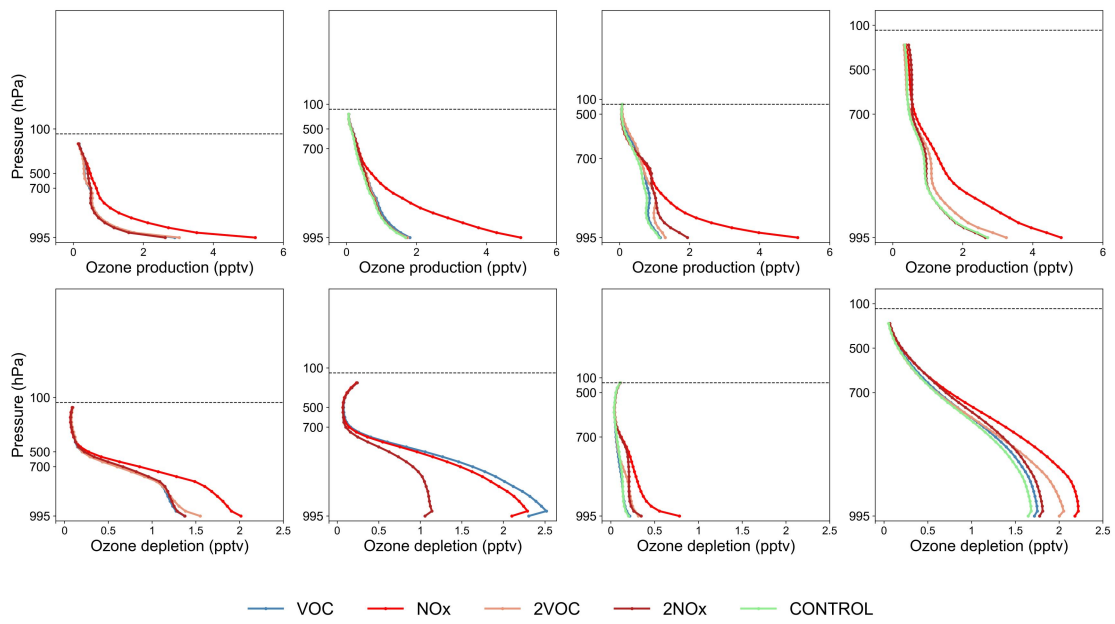
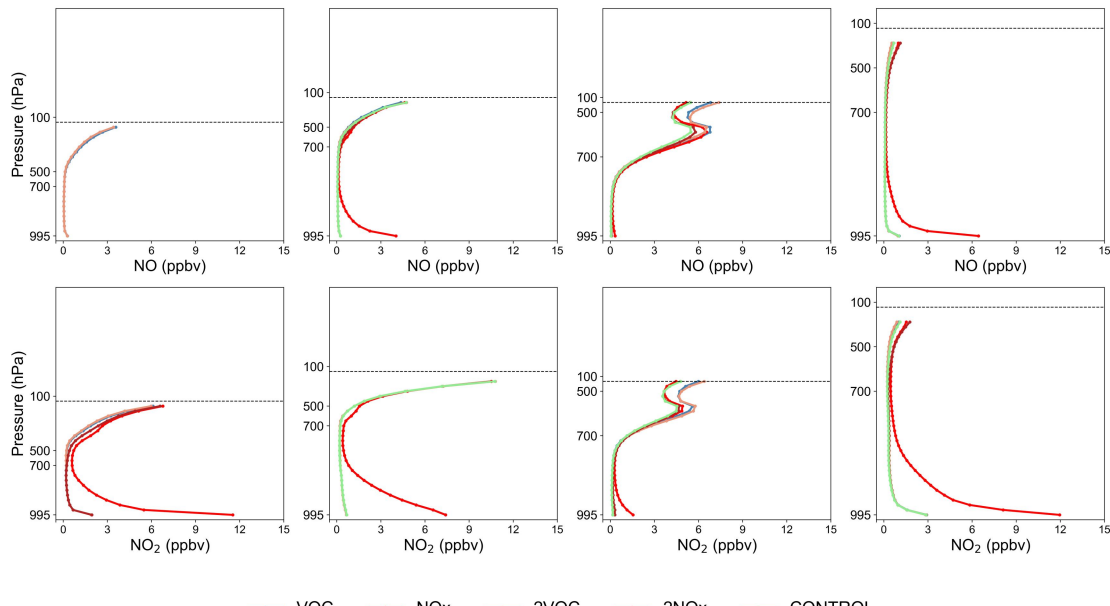


Figure 4. Vertical profiles of O₃ volume mixing ratio (a) chemical production and (b) chemical depletion rate for the 30th year across five in the four models.

Figure 4b illustrates that, apart from the O₃ chemical formation mechanism, the CESM, GFDL, and UKESM models in the *PiClim-2NO_x* experiment do not accurately depict the O₃ chemical depletion process induced by NO_x. Despite successfully replicating the rise in NO and NO₂ levels (Fig. 5a, b) in the upper troposphere, these models fall short in capturing the NO_x-related O₃ depletion phenomenon. Moreover, the GISS model stands out with notably elevated NO_x volume mixing ratios attributed to heightened lightning activity compared to the

450 other models. Additionally, it demonstrates a peak NO_x volume mixing ratio near
 451 500 hPa across all experiments conducted, a feature not observed in the other
 452 models.

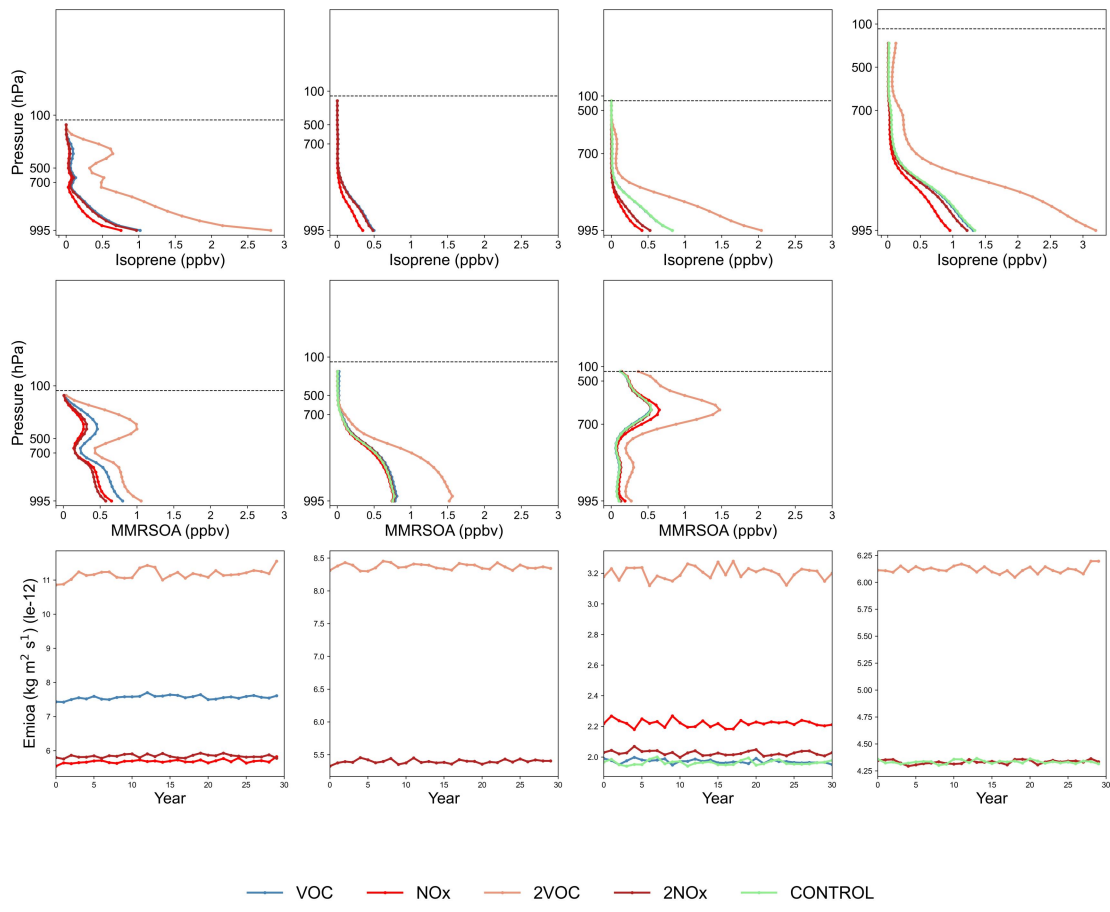
453



454
 455 **Figure 5.** Vertical profiles of (a) NO and (b) NO₂ volume mixing ratios for the 30th
 456 year across five experiments in the four models.

457 Figure 6 illustrates a notable inverse correlation between the consumption of
 458 isoprene and the chemical production of O₃ in four models, when the rise in VOCs
 459 emissions is not factored in. This relationship is attributed to the significance of
 460 isoprene as a natural VOC source in unpolluted atmospheres and highlights the
 461 absence of O₃ generation simulation due to lightning activity in the CESM, GFDL,
 462 and UKESM models. In the *PiClim* experiments, the UKESM model did not provide
 463 mass fraction of secondary particulate organic matter dry aerosol particles in the air
 464 (mmrsoa), and so we only include its volume mixing ratio of isoprene in the air
 465 (isop) and the primary emissions and chemical production of dry aerosol organic
 466 matter (emioa) in Fig. 6. Additionally, the CESM model exhibits higher emissions
 467 and chemical formation of organic dry aerosol particles compared to the GFDL and
 468 GISS models. This difference potentially contributes to the observed variation in
 469 global O₃ volume mixing ratios, with the highest levels recorded in the CESM
 470 model and the lowest in the GISS model.

471



472

473
474
475
476
477

Figure 6. Vertical profiles of (a) isoprene volume mixing ratio and (b) secondary organic aerosol mass mixing ratio for the 30th year of all available experiments across the three models. (c) Temporal evolution characteristics of major emissions and the chemical production of organic dry aerosol particles from five experiments of the four models.

478

4. Conclusions

479
480
481
482
483
484
485
486
487
488
489
490

This study assessed the sensitivity of global-scale ozone (O_3) to precursor gases in a clean atmosphere and evaluated the simulation capabilities of four Earth system models using data from the *PiClim* experiments within the AerChemMIP framework. Our results highlight both strengths and limitations of these models in capturing O_3 dynamics. The CESM and GFDL models excelled in reproducing seasonal O_3 cycles and the vertical distribution of O_3 , but they showed limitations in simulating the tropospheric O_3 response to NO_x emissions from natural sources, such as lightning activity. Conversely, the GISS and UKESM models effectively simulated the positive correlation between tropospheric O_3 and temperature but were less sensitive to natural precursors compared to anthropogenic sources. Discrepancies, such as zonal temperature biases in the GISS model and stratospheric temperature inconsistencies in the GFDL model, underscore areas for improvement.

491 Our findings suggest that existing assumptions regarding O₃ sensitivity to
492 natural precursors may require refinement in clean atmospheric conditions. This
493 research provides critical insights into the interplay between O₃ and its precursors,
494 enhancing the accuracy of O₃ simulations in Earth system models. Given the
495 significant role of O₃ in radiative forcing, atmospheric oxidation, and climate
496 feedback mechanisms, our study reinforces the necessity of precise modeling to
497 better predict and mitigate future climate scenarios. Additionally, the results
498 underscore the importance of controlling anthropogenic precursor emissions as an
499 essential strategy to manage tropospheric O₃ volume mixing ratios and address
500 broader climate change challenges.

501 It is important to acknowledge that the results generated by the models are
502 accompanied by a degree of uncertainty. Variations in the methodologies employed
503 by different models to address chemical reactions, including the production and
504 depletion of ozone, contribute to the uncertainty surrounding the ozone budget.
505 Furthermore, discrepancies in the data pertaining to anthropogenic and natural
506 emissions, particularly concerning NO_x and BVOC emissions, substantially
507 influence the outcomes of these models. Additionally, the uncertainty associated
508 with the stratosphere-troposphere exchange process represents a critical factor in the
509 ozone budget, with notable divergences in the treatment of this process across
510 various models.

511 **Acknowledgement**

512 We acknowledge the World Climate Research Programme, which, through its
513 Working Group on Coupled Modelling, coordinated and promoted CMIP6. We
514 thank the climate modelling groups for producing and making available their model
515 output, the Earth System Grid Federation (ESGF) for archiving the data and
516 providing access, and the multiple funding agencies who support CMIP6 and ESGF.
517 We acknowledge the AerChemMIP groups of the four models used in the study
518 (Vaishali Naik and Larry Horowitz for the GFDL simulations, Susanne E. Bauer
519 and Kostas Tsigaridis for the GISS simulations, Fiona O'Connor and Jonny
520 Williams for the UKESM simulations, as well as Louisa K. Emmons for the NCAR
521 simulations). Particularly, we are grateful to Dr. Vaishali Naik for her comments
522 and suggestions during the revision of this manuscript.

523 **Data availability**

524 All data from the Earth system models used in this paper are available on the
525 Earth System Grid Federation website and can be downloaded from
526 <https://esgf-index1.ceda.ac.uk/search/cmip6-ceda/> (last access: 4 July 2024,
527 ESGF-CEDA, 2024).

528 **Author contributions**

529 WW and CYG provided data analysis and contributed to the writing and
530 discussion of this paper.

531 **Competing interests**

532 The authors declare that they have no conflict of interest.

533 **References**

534 Archibald, A. T., O'Connor, F. M., Abraham, N. L., Archer-Nicholls, S.,
535 Chipperfield, M. P., Dalvi, M., Folberth, G. A., Dennison, F., Dhomse, S. S.,
536 Griffiths, P. T., Hardacre, C., Hewitt, A. J., Hill, R. S., Johnson, C. E., Keeble, J.,
537 Kohler, M. O., Morgenstern, O., Mulcahy, J. P., Ordonez, C., Pope, R. J., Rumbold,
538 S. T., Russo, M. R., Savage, N. H., Sellar, A., Stringer, M., Turnock, S. T., Wild, O.,
539 and Zeng, G.: Description and evaluation of the UKCA stratosphere-troposphere
540 chemistry scheme (StratTrop vn 1.0) implemented in UKESM1, Geoscientific
541 Model Development, 13, 1223-1266, 10.5194/gmd-13-1223-2020, 2020.
542 Austin, J., Horowitz, L. W., Schwarzkopf, M. D., Wilson, R. J., and Levy, H., II: Stratospheric Ozone and Temperature Simulated from the Preindustrial Era to the
543 Present Day, Journal of Climate, 26, 3528-3543, 10.1175/jcli-d-12-00162.1, 2013.
544 Bauer, S. E., Tsigaridis, K., Faluvegi, G., Kelley, M., Lo, K. K., Miller, R. L.,
545 Nazarenko, L., Schmidt, G. A., and Wu, J.: Historical (1850-2014) Aerosol
546 Evolution and Role on Climate Forcing Using the GISS ModelE2.1 Contribution to
547 CMIP6, Journal of Advances in Modeling Earth Systems, 12,
548 10.1029/2019ms001978, 2020.
549 Brown, F., Folberth, G. A., Sitch, S., Bauer, S., Bauters, M., Boeckx, P., Cheesman,
550 A. W., Deushi, M., Dos Santos, I., Galy-Lacaux, C., Haywood, J., Keeble, J.,
551 Mercado, L. M., O'Connor, F. M., Oshima, N., Tsigaridis, K., and Verbeeck, H.: The ozone-climate penalty over South America and Africa by 2100, Atmospheric
552 Chemistry and Physics, 22, 12331-12352, 10.5194/acp-22-12331-2022, 2022.
553 Carrillo-Torres, E. R., Hernandez-Paniagua, I. Y., and Mendoza, A.: Use of
554 Combined Observational-and Model-Derived Photochemical Indicators to Assess
555 the O₃-NO_x-VOC System Sensitivity in Urban Areas, Atmosphere, 8,
556 10.3390/atmos8020022, 2017.
557 Coffman, E., Rappold, A. G., Nethery, R. C., Anderton, J., Amend, M., Jackson, M.
558 A., Roman, H., Fann, N., Baker, K. R., and Sacks, J. D.: Quantifying Multipollutant

561 Health Impacts Using the Environmental Benefits Mapping and Analysis
562 Program-Community Edition (BenMAP-CE): A Case Study in Atlanta, Georgia,
563 *Environ Health Perspect*, 132, 37003, 10.1289/EHP12969, 2024.

564 Collins, W. J., Lamarque, J.-F., Schulz, M., Boucher, O., Eyring, V., Hegglin, M. I.,
565 Maycock, A., Myhre, G., Prather, M., Shindell, D., and Smith, S. J.: AerChemMIP:
566 quantifying the effects of chemistry and aerosols in CMIP6, *Geoscientific Model
567 Development*, 10, 585-607, 10.5194/gmd-10-585-2017, 2017.

568 Dunne, J. P., Horowitz, L. W., Adcroft, A. J., Ginoux, P., Held, I. M., John, J. G.,
569 Krasting, J. P., Malyshev, S., Naik, V., Paulot, F., Shevliakova, E., Stock, C. A.,
570 Zadeh, N., Balaji, V., Blanton, C., Dunne, K. A., Dupuis, C., Durachta, J., Dussin,
571 R., Gauthier, P. P. G., Griffies, S. M., Guo, H., Hallberg, R. W., Harrison, M., He, J.,
572 Hurlin, W., McHugh, C., Menzel, R., Milly, P. C. D., Nikonorov, S., Paynter, D. J.,
573 Ploshay, J., Radhakrishnan, A., Rand, K., Reichl, B. G., Robinson, T., Schwarzkopf,
574 D. M., Sentman, L. T., Underwood, S., Vahlenkamp, H., Winton, M., Wittenberg, A.
575 T., Wyman, B., Zeng, Y., and Zhao, M.: The GFDL Earth System Model Version
576 4.1 (GFDL-ESM 4.1): Overall Coupled Model Description and Simulation
577 Characteristics, *Journal of Advances in Modeling Earth Systems*, 12,
578 10.1029/2019ms002015, 2020.

579 Fowler, D., Pilegaard, K., Sutton, M. A., Ambus, P., Raivonen, M., Duyzer, J.,
580 Simpson, D., Fagerli, H., Fuzzi, S., Schjoerring, J. K., Granier, C., Neftel, A.,
581 Isaksen, I. S. A., Laj, P., Maione, M., Monks, P. S., Burkhardt, J., Daemgen, U.,
582 Neirynck, J., Personne, E., Wichink-Kruit, R., Butterbach-Bahl, K., Flechard, C.,
583 Tuovinen, J. P., Coyle, M., Gerosa, G., Loubet, B., Altimir, N., Gruenhage, L.,
584 Ammann, C., Cieslik, S., Paoletti, E., Mikkelsen, T. N., Ro-Poulsen, H., Cellier, P.,
585 Cape, J. N., Horvath, L., Loreto, F., Niinemets, U., Palmer, P. I., Rinne, J., Misztal,
586 P., Nemitz, E., Nilsson, D., Pryor, S., Gallagher, M. W., Vesala, T., Skiba, U.,
587 Bruegemann, N., Zechmeister-Boltenstern, S., Williams, J., O'Dowd, C., Facchini,
588 M. C., de Leeuw, G., Flossman, A., Chaumerliac, N., and Erisman, J. W.:
589 Atmospheric composition change: Ecosystems-Atmosphere interactions,
590 *Atmospheric Environment*, 43, 5193-5267, 10.1016/j.atmosenv.2009.07.068, 2009.

591 Gettelman, A., Hannay, C., Bacmeister, J. T., Neale, R. B., Pendergrass, A. G.,
592 Danabasoglu, G., Lamarque, J. F., Fasullo, J. T., Bailey, D. A., Lawrence, D. M.,
593 and Mills, M. J.: High Climate Sensitivity in the Community Earth System Model
594 Version 2 (CESM2), *Geophysical Research Letters*, 46, 8329-8337,
595 10.1029/2019gl083978, 2019.

596 Griffiths, P. T., Murray, L. T., Zeng, G., Shin, Y. M., Abraham, N. L., Archibald, A.
597 T., Deushi, M., Emmons, L. K., Galbally, I. E., Hassler, B., Horowitz, L. W.,
598 Keeble, J., Liu, J., Moeini, O., Naik, V., O'Connor, F. M., Oshima, N., Tarasick, D.,
599 Tilmes, S., Turnock, S. T., Wild, O., Young, P. J., and Zanis, P.: Tropospheric
600 ozone in CMIP6 simulations, *Atmospheric Chemistry and Physics*, 21, 4187-4218,
601 10.5194/acp-21-4187-2021, 2021.

602 Guenther, A., Hewitt, C. N., Erickson, D., Fall, R., Geron, C., Graedel, T., Harley,
603 P., Klinger, L., Lerdau, M., Mckay, W. A., Pierce, T., Scholes, B., Steinbrecher, R.,
604 Tallamraju, R., Taylor, J., and Zimmerman, P.: A global model of natural volatile
605 organic compound emissions, 100, 8873-8892, <https://doi.org/10.1029/94JD02950>,
606 1995.

607 Guenther, A. B., Jiang, X., Heald, C. L., Sakulyanontvittaya, T., Duhl, T., Emmons,
608 L. K., and Wang, X.: The Model of Emissions of Gases and Aerosols from Nature
609 version 2.1 (MEGAN2.1): an extended and updated framework for modeling
610 biogenic emissions, *Geoscientific Model Development*, 5, 1471-1492,
611 10.5194/gmd-5-1471-2012, 2012.

612 Hakim, Z. Q., Archer-Nicholls, S., Beig, G., Folberth, G. A., Sudo, K., Abraham, N.
613 L., Ghude, S., Henze, D. K., and Archibald, A. T.: Evaluation of tropospheric ozone
614 and ozone precursors in simulations from the HTAPII and CCMI model
615 intercomparisons - a focus on the Indian subcontinent, *Atmospheric Chemistry and
616 Physics*, 19, 6437-6458, 10.5194/acp-19-6437-2019, 2019.

617 Hamlin, A. J. and Honrath, R. E. J. J. o. G. R.: A modeling study of the impact of
618 winter–spring arctic outflow on the NO_x and O₃ budgets of the North Atlantic
619 troposphere, 107, 2002.

620 Horowitz, L. W., Naik, V., Paulot, F., Ginoux, P. A., Dunne, J. P., Mao, J., Schnell,
621 J., Chen, X., He, J., John, J. G., Lin, M., Lin, P., Malyshev, S., Paynter, D.,
622 Shevliakova, E., and Zhao, M.: The GFDL Global Atmospheric Chemistry-Climate
623 Model AM4.1: Model Description and Simulation Characteristics, *Journal of
624 Advances in Modeling Earth Systems*, 12, 10.1029/2019ms002032, 2020.

625 Hu, L., Wang, Z., Huang, M., Sun, H., and Wang, Q.: A remote sensing based
626 method for assessing the impact of O₃ on the net primary productivity
627 of terrestrial ecosystems in China, *Frontiers in Environmental Science*, 11,
628 10.3389/fenvs.2023.1112874, 2023.

629 Jin, X., Fiore, A. M., and Cohen, R. C.: Space-Based Observations of Ozone
630 Precursors within California Wildfire Plumes and the Impacts on Ozone-NO_x-VOC
631 Chemistry, *Environmental Science & Technology*, 57, 14648-14660,
632 10.1021/acs.est.3c04411, 2023.

633 Karl, T., Lamprecht, C., Graus, M., Cede, A., Tiefengraber, M., de Arellano, J.
634 V.-G., Gurarie, D., and Lenschow, D.: High urban NO_x triggers a substantial
635 chemical downward flux of ozone, *Science Advances*, 9, 10.1126/sciadv.add2365,
636 2023.

637 Karset, I. H. H., Berntsen, T. K., Storelvmo, T., Alterskjaer, K., Grini, A., Olivie, D.,
638 Kirkevag, A., Seland, O., Iversen, T., and Schulz, M.: Strong impacts on aerosol
639 indirect effects from historical oxidant changes, *Atmospheric Chemistry and
640 Physics*, 18, 7669-7690, 10.5194/acp-18-7669-2018, 2018.

641 Kelley, M., Schmidt, G. A., Nazarenko, L. S., Bauer, S. E., Ruedy, R., Russell, G.
642 L., Ackerman, A. S., Aleinov, I., Bauer, M., Bleck, R., Canuto, V., Cesana, G.,
643 Cheng, Y., Clune, T. L., Cook, B. I., Cruz, C. A., Del Genio, A. D., Elsaesser, G. S.,
644 Faluvegi, G., Kiang, N. Y., Kim, D., Lacis, A. A., Leboissetier, A., LeGrande, A. N.,
645 Lo, K. K., Marshall, J., Matthews, E. E., McDermid, S., Mezuman, K., Miller, R. L.,
646 Murray, L. T., Oinas, V., Orbe, C., Perez Garcia-Pando, C., Perlitz, J. P., Puma, M.
647 J., Rind, D., Romanou, A., Shindell, D. T., Sun, S., Tausnev, N., Tsigaridis, K.,
648 Tselioudis, G., Weng, E., Wu, J., and Yao, M.-S.: GISS-E2.1: Configurations and
649 Climatology, *Journal of Advances in Modeling Earth Systems*, 12,
650 10.1029/2019ms002025, 2020.

651 Khomsi, K., Chelhaoui, Y., Alilou, S., Souri, R., Najmi, H., and Souhaili, Z.:
652 Concurrent Heat Waves and Extreme Ozone (O₃) Episodes: Combined

653 Atmospheric Patterns and Impact on Human Health, International Journal of
654 Environmental Research and Public Health, 19, 10.3390/ijerph19052770, 2022.

655 Kumaş, K., Akyüz, A. J. I. J. o. E., and Geoinformatics: Estimation of Greenhouse
656 Gas Emission and Global Warming Potential of Livestock Sector; Lake District,
657 Türkiye, 2023.

658 Li, M., Huang, X., Yan, D., Lai, S., Zhang, Z., Zhu, L., Lu, Y., Jiang, X., Wang, N.,
659 Wang, T., Song, Y., and Ding, A.: Coping with the concurrent heatwaves and ozone
660 extremes in China under a warming climate, Science Bulletin, 69, 2938-2947,
661 <https://doi.org/10.1016/j.scib.2024.05.034>, 2024.

662 Lim, C. C., Hayes, R. B., Ahn, J., Shao, Y., Silverman, D. T., Jones, R. R., Garcia,
663 C., Bell, M. L., and Thurston, G. D.: Long-Term Exposure to Ozone and
664 Cause-Specific Mortality Risk in the United States, American Journal of
665 Respiratory and Critical Care Medicine, 200, 1022-1031,
666 10.1164/rccm.201806-1161OC, 2019.

667 Malley, C. S., Henze, D. K., Kuylenstierna, J. C. I., Vallack, H. W., Davila, Y.,
668 Anenberg, S. C., Turner, M. C., and Ashmore, M. R.: Updated Global Estimates of
669 Respiratory Mortality in Adults \geq 30 Years of Age Attributable to Long-Term
670 Ozone Exposure, Environ Health Perspect, 125, 087021, 10.1289/EHP1390, 2017.

671 Miller, R. L., Schmidt, G. A., Nazarenko, L. S., Tausnev, N., Bauer, S. E., DelGenio,
672 A. D., Kelley, M., Lo, K. K., Ruedy, R., Shindell, D. T., Aleinov, I., Bauer, M.,
673 Bleck, R., Canuto, V., Chen, Y., Cheng, Y., Clune, T. L., Faluvegi, G., Hansen, J. E.,
674 Healy, R. J., Kiang, N. Y., Koch, D., Lacis, A. A., LeGrande, A. N., Lerner, J.,
675 Menon, S., Oinas, V., Garcia-Pando, C. P., Perlitz, J. P., Puma, M. J., Rind, D.,
676 Romanou, A., Russell, G. L., Sato, M., Sun, S., Tsigaridis, K., Unger, N.,
677 Voulgarakis, A., Yao, M.-S., and Zhang, J.: CMIP5 historical simulations
678 (1850-2012) with GISS ModelE2, Journal of Advances in Modeling Earth Systems,
679 6, 441-477, 10.1002/2013ms000266, 2014.

680 Möller, D. and Mauersberger, G.: Cloud chemistry effects on tropospheric
681 photooxidants in polluted atmosphere — Model results, Journal of Atmospheric
682 Chemistry, 14, 153-165, 10.1007/BF00115231, 1992.

683 Monks, P. S., Archibald, A. T., Colette, A., Cooper, O., Coyle, M., Derwent, R.,
684 Fowler, D., Granier, C., Law, K. S., Mills, G. E., Stevenson, D. S., Tarasova, O.,
685 Thouret, V., von Schneidemesser, E., Sommariva, R., Wild, O., and Williams, M. L.:
686 Tropospheric ozone and its precursors from the urban to the global scale from air
687 quality to short-lived climate forcer, Atmospheric Chemistry and Physics, 15,
688 8889-8973, 10.5194/acp-15-8889-2015, 2015.

689 Mulcahy, J. P., Jones, C., Sellar, A., Johnson, B., Boutle, I. A., Jones, A., Andrews,
690 T., Rumbold, S. T., Mollard, J., Bellouin, N., Johnson, C. E., Williams, K. D.,
691 Grosvenor, D. P., and McCoy, D. T.: Improved Aerosol Processes and Effective
692 Radiative Forcing in HadGEM3 and UKESM1, Journal of Advances in Modeling
693 Earth Systems, 10, 2786-2805, 10.1029/2018ms001464, 2018.

694 Murray, L. T., Logan, J. A., and Jacob, D. J.: Interannual variability in tropical
695 tropospheric ozone and OH: The role of lightning, 118, 11,468-411,480,
696 <https://doi.org/10.1002/jgrd.50857>, 2013.

697 Naik, V., Horowitz, L. W., Fiore, A. M., Ginoux, P., Mao, J., Aghedo, A. M., and
698 Levy, H., II: Impact of preindustrial to present-day changes in short-lived pollutant

699 emissions on atmospheric composition and climate forcing, *Journal of Geophysical*
700 *Research-Atmospheres*, 118, 8086-8110, 10.1002/jgrd.50608, 2013a.

701 Naik, V., Voulgarakis, A., Fiore, A. M., Horowitz, L. W., Lamarque, J. F., Lin, M.,
702 Prather, M. J., Young, P. J., Bergmann, D., Cameron-Smith, P. J., Cionni, I., Collins,
703 W. J., Dalsøren, S. B., Doherty, R., Eyring, V., Faluvegi, G., Folberth, G. A., Josse,
704 B., Lee, Y. H., MacKenzie, I. A., Nagashima, T., van Noije, T. P. C., Plummer, D.
705 A., Righi, M., Rumbold, S. T., Skeie, R., Shindell, D. T., Stevenson, D. S., Strode,
706 S., Sudo, K., Szopa, S., and Zeng, G.: Preindustrial to present-day changes in
707 tropospheric hydroxyl radical and methane lifetime from the Atmospheric
708 Chemistry and Climate Model Intercomparison Project (ACCMIP), *Atmos. Chem.*
709 *Phys.*, 13, 5277-5298, 10.5194/acp-13-5277-2013, 2013b.

710 Nuvolone, D., Petri, D., and Voller, F.: The effects of ozone on human health,
711 *Environ Sci Pollut Res Int*, 25, 8074-8088, 10.1007/s11356-017-9239-3, 2018.

712 Pacifico, F., Harrison, S. P., Jones, C. D., Arneth, A., Sitch, S., Weedon, G. P.,
713 Barkley, M. P., Palmer, P. I., Serca, D., Potosnak, M., Fu, T. M., Goldstein, A., Bai,
714 J., and Schurgers, G.: Evaluation of a photosynthesis-based biogenic isoprene
715 emission scheme in JULES and simulation of isoprene emissions under present-day
716 climate conditions, *Atmospheric Chemistry and Physics*, 11, 4371-4389,
717 10.5194/acp-11-4371-2011, 2011.

718 Price, C. and Rind, D.: A simple lightning parameterization for calculating global
719 lightning distributions, 97, 9919-9933, <https://doi.org/10.1029/92JD00719>, 1992.

720 Price, C., Penner, J., and Prather, M.: NO_x from lightning: 1. Global distribution
721 based on lightning physics, 102, 5929-5941, <https://doi.org/10.1029/96JD03504>,
722 1997.

723 Price, C. G.: Lightning Applications in Weather and Climate Research, *Surveys in*
724 *Geophysics*, 34, 755-767, 10.1007/s10712-012-9218-7, 2013.

725 Rogelj, J., Schaeffer, M., Meinshausen, M., Shindell, D. T., Hare, W., Klimont, Z.,
726 Velders, G. J. M., Amann, M., and Schellnhuber, H. J.: Disentangling the effects of
727 CO₂ and short-lived climate forcer mitigation, *Proceedings of the*
728 *National Academy of Sciences of the United States of America*, 111, 16325-16330,
729 10.1073/pnas.1415631111, 2014.

730 Schnell, J. L., Naik, V., Horowitz, L. W., Paulot, F., Mao, J., Ginoux, P., Zhao, M.,
731 and Ram, K.: Exploring the relationship between surface PM_{2.5} and
732 meteorology in Northern India, *Atmospheric Chemistry and Physics*, 18,
733 10157-10175, 10.5194/acp-18-10157-2018, 2018.

734 Sellar, A. A., Jones, C. G., Mulcahy, J. P., Tang, Y., Yool, A., Wiltshire, A.,
735 O'Connor, F. M., Stringer, M., Hill, R., Palmieri, J., Woodward, S., de Mora, L.,
736 Kuhlbrodt, T., Rumbold, S. T., Kelley, D. I., Ellis, R., Johnson, C. E., Walton, J.,
737 Abraham, N. L., Andrews, M. B., Andrews, T., Archibald, A. T., Berthou, S., Burke,
738 E., Blockley, E., Carslaw, K., Dalvi, M., Edwards, J., Folberth, G. A., Gedney, N.,
739 Griffiths, P. T., Harper, A. B., Hendry, M. A., Hewitt, A. J., Johnson, B., Jones, A.,
740 Jones, C. D., Keeble, J., Liddicoat, S., Morgenstern, O., Parker, R. J., Predoi, V.,
741 Robertson, E., Siahaan, A., Smith, R. S., Swaminathan, R., Woodhouse, M. T.,
742 Zeng, G., and Zerroukat, M.: UKESM1: Description and Evaluation of the UK
743 Earth System Model, *Journal of Advances in Modeling Earth Systems*, 11,
744 4513-4558, 10.1029/2019ms001739, 2019.

745 Shindell, D. T., Faluvegi, G., Unger, N., Aguilar, E., Schmidt, G. A., Koch, D. M.,
746 Bauer, S. E., and Miller, R. L.: Simulations of preindustrial, present-day, and 2100
747 conditions in the NASA GISS composition and climate model G-PUCCINI,
748 Atmospheric Chemistry and Physics, 6, 4427-4459, 10.5194/acp-6-4427-2006,
749 2006.

750 Shindell, D. T., Pechony, O., Voulgarakis, A., Faluvegi, G., Nazarenko, L.,
751 Lamarque, J. F., Bowman, K., Milly, G., Kovari, B., Ruedy, R., and Schmidt, G. A.:
752 Interactive ozone and methane chemistry in GISS-E2 historical and future climate
753 simulations, Atmospheric Chemistry and Physics, 13, 2653-2689,
754 10.5194/acp-13-2653-2013, 2013.

755 Sillman, S. and He, D.: Some theoretical results concerning O₃-NO_x-VOC
756 chemistry and NO_x-VOC indicators, 107, ACH 26-21-ACH 26-15,
757 <https://doi.org/10.1029/2001JD001123>, 2002.

758 Sporre, M. K., Blichner, S. M., Karset, I. H. H., Makkonen, R., and Berntsen, T. K.:
759 BVOC-aerosol-climate feedbacks investigated using NorESM, Atmospheric
760 Chemistry and Physics, 19, 4763-4782, 10.5194/acp-19-4763-2019, 2019.

761 Stevenson, D. S., Young, P. J., Naik, V., Lamarque, J. F., Shindell, D. T.,
762 Voulgarakis, A., Skeie, R. B., Dalsoren, S. B., Myhre, G., Berntsen, T. K., Folberth,
763 G. A., Rumbold, S. T., Collins, W. J., MacKenzie, I. A., Doherty, R. M., Zeng, G.,
764 van Noije, T. P. C., Strunk, A., Bergmann, D., Cameron-Smith, P., Plummer, D. A.,
765 Strode, S. A., Horowitz, L., Lee, Y. H., Szopa, S., Sudo, K., Nagashima, T., Josse,
766 B., Cionni, I., Righi, M., Eyring, V., Conley, A., Bowman, K. W., Wild, O., and
767 Archibald, A.: Tropospheric ozone changes, radiative forcing and attribution to
768 emissions in the Atmospheric Chemistry and Climate Model Intercomparison
769 Project (ACCMIP), Atmospheric Chemistry and Physics, 13, 3063-3085,
770 10.5194/acp-13-3063-2013, 2013.

771 Stevenson, D. S., Dentener, F. J., Schultz, M. G., Ellingsen, K., van Noije, T. P. C.,
772 Wild, O., Zeng, G., Amann, M., Atherton, C. S., Bell, N., Bergmann, D. J., Bey, I.,
773 Butler, T., Cofala, J., Collins, W. J., Derwent, R. G., Doherty, R. M., Drevet, J.,
774 Eskes, H. J., Fiore, A. M., Gauss, M., Hauglustaine, D. A., Horowitz, L. W., Isaksen,
775 I. S. A., Krol, M. C., Lamarque, J. F., Lawrence, M. G., Montanaro, V., Müller, J. F.,
776 Pitari, G., Prather, M. J., Pyle, J. A., Rast, S., Rodriguez, J. M., Sanderson, M. G.,
777 Savage, N. H., Shindell, D. T., Strahan, S. E., Sudo, K., and Szopa, S.: Multimodel
778 ensemble simulations of present-day and near-future tropospheric ozone, Journal of
779 Geophysical Research-Atmospheres, 111, 10.1029/2005jd006338, 2006.

780 Tilmes, S., Visioni, D., Jones, A., Haywood, J., Seferian, R., Nabat, P., Boucher, O.,
781 Bednarz, E. M., and Niemeier, U.: Stratospheric ozone response to sulfate aerosol
782 and solar dimming climate interventions based on the G6 Geoengineering Model
783 Intercomparison Project (GeoMIP) simulations, Atmospheric Chemistry and
784 Physics, 22, 4557-4579, 10.5194/acp-22-4557-2022, 2022.

785 Unger, N.: On the role of plant volatiles in anthropogenic global climate change, 41,
786 8563-8569, <https://doi.org/10.1002/2014GL061616>, 2014.

787 van Marle, M. J. E., Kloster, S., Magi, B. I., Marlon, J. R., Daniau, A. L., Field, R.
788 D., Arneth, A., Forrest, M., Hantson, S., Kehrwald, N. M., Knorr, W., Lasslop, G.,
789 Li, F., Mangeon, S., Yue, C., Kaiser, J. W., and van der Werf, G. R.: Historic global
790 biomass burning emissions for CMIP6 (BB4CMIP) based on merging satellite

791 observations with proxies and fire models (1750–2015), *Geosci. Model Dev.*, 10,
792 3329-3357, 10.5194/gmd-10-3329-2017, 2017.

793 Vermeuel, M. P., Novak, G. A., Alwe, H. D., Hughes, D. D., Kaleel, R. J., Dickens,
794 A., Kenski, D., Czarnetzki, A. C., Stone, E. A., Stanier, C. O., Pierce, R. B., Millet,
795 D. B., and Bertram, T. H. J. J. o. G. R. A.: Sensitivity of Ozone Production to NO_x
796 and VOC Along the Lake Michigan Coastline, 124, 10989 - 11006, 2019.

797 Walters, D., Baran, A. J., Boutle, I., Brooks, M., Earnshaw, P., Edwards, J., Furtado,
798 K., Hi, P., Lock, A., Manners, J., Morcrette, C., Mulcahy, J., Sanchez, C., Smith, C.,
799 Stratton, R., Tennant, W., Tomassini, L., Van Weverberg, K., Vosper, S., Willett,
800 M., Browse, J., Bushell, A., Carslaw, K., Dalvi, M., Essery, R., Gedney, N.,
801 Hardiman, S., Johnson, B., Johnson, C., Jones, A., Jones, C., Mann, G., Milton, S.,
802 Rumbold, H., Sellar, A., Ujiie, M., Whitall, M., Williams, K., and Zerroukat, M.:
803 The Met Office Unified Model Global Atmosphere 7.0/7.1 and JULES Global Land
804 7.0 configurations, *Geoscientific Model Development*, 12, 1909-1963,
805 10.5194/gmd-12-1909-2019, 2019.

806 Williams, K. D., Copsey, D., Blockley, E. W., Bodas-Salcedo, A., Calvert, D.,
807 Comer, R., Davis, P., Graham, T., Hewitt, H. T., Hill, R., Hyder, P., Ineson, S.,
808 Johns, T. C., Keen, A. B., Lee, R. W., Megann, A., Milton, S. F., Rae, J. G. L.,
809 Roberts, M. J., Scaife, A. A., Schiemann, R., Storkey, D., Thorpe, L., Watterson, I.
810 G., Walters, D. N., West, A., Wood, R. A., Woollings, T., and Xavier, P. K.: The
811 Met Office Global Coupled Model 3.0 and 3.1 (GC3.0 and GC3.1) Configurations,
812 *Journal of Advances in Modeling Earth Systems*, 10, 357-380,
813 10.1002/2017ms001115, 2018.

814 Young, P. J., Naik, V., Fiore, A. M., Gaudel, A., Guo, J., Lin, M. Y., Neu, J. L.,
815 Parrish, D. D., Rieder, H. E., Schnell, J. L., Tilmes, S., Wild, O., Zhang, L., Ziemke,
816 J., Brandt, J., Delcloo, A., Doherty, R. M., Geels, C., Hegglin, M. I., Hu, L., Im, U.,
817 Kumar, R., Luhar, A., Murray, L., Plummer, D., Rodriguez, J., Saiz-Lopez, A.,
818 Schultz, M. G., Woodhouse, M. T., and Zeng, G.: Tropospheric Ozone Assessment
819 Report: Assessment of global-scale model performance for global and regional
820 ozone distributions, variability, and trends, *Elementa-Science of the Anthropocene*,
821 6, 10.1525/elementa.265, 2018.

822 Zeng, G., Morgenstern, O., Williams, J. H. T., O'Connor, F. M., Griffiths, P. T.,
823 Keeble, J., Deushi, M., Horowitz, L. W., Naik, V., Emmons, L. K., Abraham, N. L.,
824 Archibald, A. T., Bauer, S. E., Hassler, B., Michou, M., Mills, M. J., Murray, L. T.,
825 Oshima, N., Sentman, L. T., Tilmes, S., Tsigaridis, K., and Young, P. J.: Attribution
826 of Stratospheric and Tropospheric Ozone Changes Between 1850 and 2014 in
827 CMIP6 Models, *Journal of Geophysical Research-Atmospheres*, 127,
828 10.1029/2022jd036452, 2022.